Journal of Materials Chemistry B

ROYAL SOCIETY OF CHEMISTRY

PAPER

View Article Online
View Journal | View Issue

Cite this: J. Mater. Chem. B, 2022, 10, 7622

Photovoltaic molecules with ultra-high light energy utilization for near-infrared laser triggered synergetic photodynamic and photothermal therapy†

Ke Yang, ‡[a] Zequn Zhang,‡[b] Yabin Gan,[c] Qiuxia Tan,[a] Li Huang,[a] Benhua Wang, [a] Gui Hu,[b] Peng Yin, [c] Xiangzhi Song [a] and Minhuan Lan *[a]

Photovoltaic molecules possess strong absorption in the near-infrared (NIR) region and are suitable for NIR laser-triggered phototherapy. Herein, the star molecule IEICO of organic photovoltaic materials, which has a narrow bandgap and large A–D–A conjugated structure, was prepared into water dispersive nanoparticles (NPs) through a simple self-assembly method. The obtained IEICO NPs showed a strong NIR absorption peak at 800 nm and a high $^1O_2$ quantum yield of 11% and photothermal conversion efficiency of 85.4% under 808 nm laser irradiation. The ultra-high light energy utilization efficacy (~96.4%) of the IEICO NPs enables their excellent phototherapeutic effect on tumors. The present work suggested the huge application potential of organic photovoltaic materials in the biomedical field.

Received 5th May 2022,
Accepted 27th June 2022

DOI: 10.1039/d2tb00984f

rsc.li/materials-b

Introduction

Traditional clinical cancer treatments, such as surgery, radiotherapy, and chemotherapy, are limited by drug resistance, severe side effects, low therapeutic efficacy, and poor tumor targetability.[1–3] Phototherapy with high selectivity and efficiency, non-invasiveness, and negligible drug resistance is becoming a promising cancer treatment strategy.[4,5] Phototherapy includes photodynamic therapy (PDT) and photothermal therapy (PTT). In PDT, photosensitizers absorb light and then produce reactive oxygen species (ROS), which can kill cells with a strong oxidative capacity;[6–8] while in PTT, photothermal agents convert the photoenergy into heat to ablate cells.[9–11] Considering the hypoxic tumor microenvironment and the presence of heat shock proteins, the combination of PDT and PTT can achieve better therapeutic efficacy.[12,13]

In addition to ROS generation capability and photothermal conversion efficiency (PCE), the wavelength of excitation light also has a great impact on the efficacy of phototherapy. Near-infrared (NIR) light with wavelengths located in biological windows has a strong tissue penetrating ability, and thus the deep cancer cells could be effectively killed by NIR laser excitation during phototherapy.[14] However, photosensitizers for clinical use, including porphyrins, hypocrellins, and phthalocyanines have a poor absorption capability in the NIR region, while the photothermal agents with strong NIR absorption, such as metal-/carbon-/semiconductor-based nanomaterials are limited by their non-biodegradability and cytotoxicity.[15–17] Therefore, the design of NIR laser triggered, biodegradable and

[a] College of Chemistry and Chemical Engineering, Central South University, Changsha, P. R. China. E-mail: minhuanlan@csu.edu.cn
[b] Department of Gastrointestinal Surgery, The Third Xiangya Hospital of Central South University, Changsha, P. R. China
[c] College of Chemistry and Chemical Engineering, Hunan Normal University, Changsha, P. R. China

† Electronic supplementary information (ESI) available. See DOI: https://doi.org/10.1039/d2tb00984f

‡ The authors contributed equally to this work.

Minhuan Lan

Minhuan Lan received his PhD degree in organic chemistry in 2013 from the Technical Institute of Physics and Chemistry, Chinese Academy of Sciences (TIPC, CAS) under the supervision of Prof. Pengfei Wang and Prof. Wenjun Zhang. Then, he joined Prof. Wenjun Zhang's group as a postdoctoral researcher at the City University of Hong Kong (from 2013 to 2017). He joined Central South University (CSU) in 2017 as a professor. His research focuses on carbon nanomaterials, chemosensors/biosensors, bioimaging, and phototherapy.

highly efficient photosensitizers or photothermal agents, especially multifunctional agents that can simultaneously generate ROS and heat with a high light energy utilization efficiency, can promote the development of phototherapy technology and the treatment of tumors.[18–20]

In recent years, researchers have made important progress in organic solar cells (OSC) based on non-fullerene electron acceptors.[21–24] IEICO, one of these electron acceptors, consists of a terminal electron acceptor group (dicyano substituted indanone unit), alkoxythiophene bridge, and core (IDT unit containing phenylalkyl side chain).[25,26] It has a narrow band gap of 1.34 eV, and its LUMO and HOMO energy levels are −3.95 and 5.06 eV, respectively, indicating a wide absorption spectrum. The large conjugated A–D–A structure is conducive to the redshift in absorption spectra and the intramolecular rotation of the flexible chain, which can guarantee strong light absorption ability and photothermal conversion ability in the NIR region.[27] The lower band gap contributes to the production of singlet oxygen, which assists PDT.[28] These properties enable the application of IEICO in the biological field.[29,30]

Herein the hydrophobic IEICO molecule was prepared into water dispersible nanoparticles (NPs) by the simple self-assembly method. The obtained IEICO NPs were proved to possess excellent photoacoustic imaging (PAI) ability, high singlet oxygen generation quantum yield (11%) and high PCE (85.4%). The ultra-high light energy utilization efficacy of 96.4% can be attributed to the unique molecular structure of IEICO, *i.e.*, the large A–D–A conjugated structure and small narrow band gap (1.34 eV).[31,32] In addition, *in vitro* experimental results revealed that the IEICO NPs have good photothermal stability and biocompatibility. Furthermore, the flow cytometry assay and phalloidin staining revealed the mechanism of how IEICO NPs induced death, and the H&E and Ki67 staining demonstrated the efficient therapeutic effect *in vivo*. Based on the outstanding performance, the huge application potential of IEICO NPs in PA imaging-guided photothermal/photodynamic combinational therapy under 808 nm laser irradiation was demonstrated.

Experimental

Materials

IEICO was purchased from Solarmer Materials Inc. Indocyanine green (ICG) was purchased from Energy Chemical. Singlet Oxygen Sensor Green (SOSG) was purchased from Dalian Meilun Biotechnology Co., Ltd. Calcein acetoxymethylester (Calcine AM) and propidium iodide (PI) were purchased from Tianjin Heans Biochemical Technology.

Instruments

UV-vis spectra were obtained by a Shimadzu UV-2600 spectrophotometer. Fluorescence spectrum spectra were measured on an RF-6000 spectrophotometer. Scanning electron microscopy (SEM) images were captured from JSM-7610F, JEOL Ltd. The fluorescence imaging was performed by Leica SP8 confocal laser scanning microscopy.

Preparation of IEICO NPs

IEICO NPs were prepared by using the nanoprecipitation method. In detail, 200 μL IEICO (500 μM, THF) were dropped into 10 mL of water under strong ultrasonication.

Calculation of photothermal conversion efficiency

η was determined according to eqn (1):

$$\eta = \frac{hA(T_{\mathrm{Max}} - T_{\mathrm{Surr}}) - Q_{\mathrm{Dis}}}{I(1 - 10^{-A_{808}})} \quad (1)$$

T_{Max} and T_{Surr} are the plateau and surrounding temperature, respectively. Q_{D} represents the heat dissipation resulted by the solvent, and I is the laser power intensity. hA was obtained from eqn (2):

$$\tau = \frac{m_{\mathrm{D}} c_{\mathrm{D}}}{hA} \quad (2)$$

m_{D} and c_{D} are the mass and heat capacity of DI water, respectively. τ_s was calculated from eqn (3):

$$t = -\tau_S \ln(\theta) = -\tau_S \ln\left(\frac{T_t - T_{\mathrm{Surr}}}{T_{\mathrm{Max}} - T_{\mathrm{Surr}}}\right) \quad (3)$$

where t is the cooling time point after continuous irradiation for 10 min, and T_t is the corresponding temperature. Q_{D} is determined according to eqn (4):

$$Q_{\mathrm{Dis}} = \frac{c_{\mathrm{D}} m_{\mathrm{D}} \left(T_{\mathrm{Max(water)}} - T_{\mathrm{Surr}}\right)}{\tau_{S(\mathrm{water})}} \quad (4)$$

According to the experiment data and above equation, η was calculated to be 85.4%.

The ROS generation of IEICO NPs

Solution level: SOSG was used to detect the generation of singlet oxygen in water solution. IEICO NPs (10 μM) were mixed with SOSG and then irradiated (808 nm, 0.02 W cm^{-2}) for 300 s. Intracellular level: DCFH-DA was added to a confocal dish, which contains 4T1 cells incubated with IEICO NPs. The confocal dishes of groups (IEICO NPs + laser and PBS + laser) were exposed to an 808 nm laser (0.5 W cm^{-2}, 10 min).

Calcein AM and PI co-staining assay

Calcein-AM (AM, 10 μg mL^{-1}, 500 μL) and propidium iodide (PI, 5 μg mL^{-1}, 500 μL) were used to stain the live cells and dead cells, respectively. The dishes were divided into four groups to detect the influence on cells of laser density, concentration of IEICO NPs and the lethal effect. After the different treatments, the cells were stained with AM and PI (conditions: [IEICO NPs] = 5 μM; [laser] = 808 nm, 1 W cm^{-2}, 10 min).

Animal model

All the conducted animal experiments were permitted by the ethics committee of Central South University. The mice (BALB/c, male, 8 weeks) were purchased from Hunan SJA Laboratory

Animal Co., Ltd. To establish the mouse tumor model, 4T1 cells were subcutaneously administered to the mice.

In vivo treatment

When the volume of 4T1 tumors grew to about 150 mm^3, we tested the *in vivo* therapeutic effect of IEICO NPs. Mice were randomly divided into four groups as the following: PBS, PBS + laser (808 nm, 1 W cm^{-2}, 10 min), IEICO NPs (10 μM) and IEICO NPs + laser (10 μM, 808 nm, 1 W cm^{-2}, 10 min). The body weight and tumor volume of the mice were measured and recorded for 14 days.

Results and discussion

The molecular structure of IEICO is presented in Fig. 1a. The hydrophobic IEICO molecule was prepared into biocompatible and water dispersible NPs through the self-assembly method.[33] The morphology and particle size distribution of IEICO NPs were characterized by Scanning Electron Microscopy (SEM). As shown in Fig. 1b and c, IEICO NPs were spherical with an average diameter of about 141 nm. The IEICO dissolved in THF solution exhibits a strong NIR absorbance peaked at 743 nm, after being prepared into NPs, the red-shift and splitting of the absorption peaked at 803 and 730 nm were observed (Fig. 1d). Here we proposed that the red-shifted absorption peaked at 803 nm is originated from the J-type aggregation of IEICO due to its distinct π–π interaction. While the split absorption peaked at 730 nm may be attributed to the intensive absorption of IEICO on the surface of NPs, which has been affected by the reduced micropolarity induced by the six alkyl hydrophobic chains of the IEICO.[34–37] The obtained IEICO NPs exhibited excellent stability. As shown in Fig. S1 (ESI†), the absorption spectra and size distribution showed no obvious changes after 7 days, suggesting that the IEICO NPs could be stored for at least one week in air at room temperature.

Since the absorption peak was located at 808 nm, the photothermal conversion capability of IEICO NPs was studied using an 808 nm laser. Fig. 2a shows the time-dependent temperature variation of the IEICO NP aqueous solution with

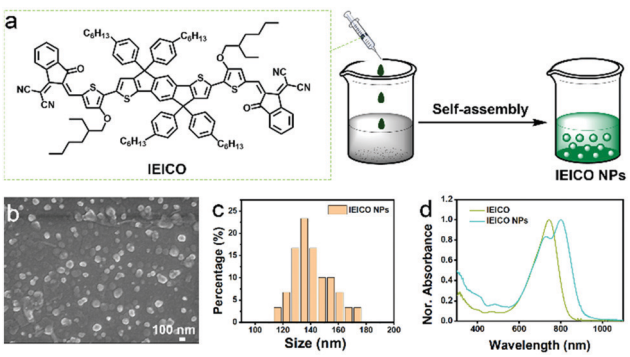

Fig. 1 (a) The molecular structure of IEICO and the preparation of IEICO NPs. (b) SEM image. (c) Particle size distribution histograms of IEICO NPs. (d) The normalized absorbance spectrum of IEICO in THF and IEICO NPs in water.

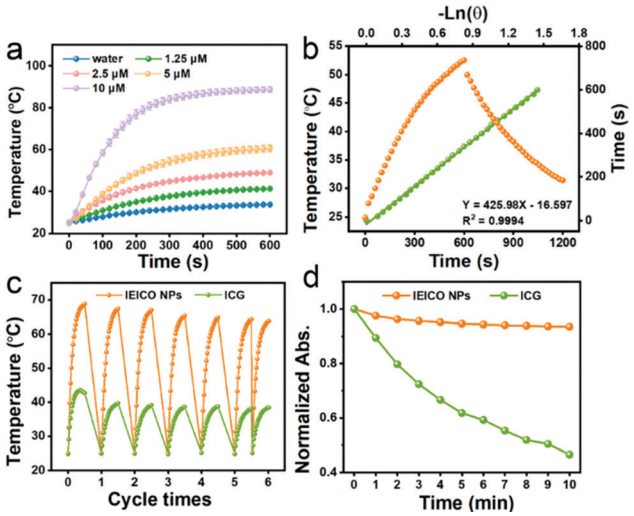

Fig. 2 (a) Time-dependent temperature variation of IEICO NP aqueous solutions with different concentrations under 808 nm laser irradiation (1 W cm^{-2}). (b) Photothermal conversion efficiency of IEICO NPs. (c) The temperature changes of IEICO NPs (10 μM) and ICG (10 μM) in aqueous solutions under 808 nm laser for 6 cycles. (d) Time-dependent normalized absorbance of IEICO NPs and ICG.

different concentrations under 808 nm laser irradiation. Increasing the concentration of IEICO NPs, or prolonging the irradiation time will increase the temperature rapidly. In the presence of 5 μM IEICO NPs, the temperature was increased to ~60 °C after 10 min laser irradiation, which is high enough to ablate cancer cells, while in the group without IEICO NPs or IEICO (5 μM) in toluene (Fig. S2, ESI†), under the same laser irradiation conditions, the temperature was only increased to 34 °C and 42 °C respectively, demonstrating the excellent photothermal conversion capability of the IEICO NPs. The PCE of IEICO NPs was calculated to be 85.4% based on the temperature rising and cooling curves of IEICO NPs (Fig. 2b), which is much higher than that of previously reported photothermal agents (listed in Table S1, ESI†). Moreover, the IEICO NPs also showed better photostability than the clinically used photosensitizer, indocyanine green (ICG). As shown in Fig. 2c, the temperature of the IEICO NP solution could still increase to ~63.8 °C after 6 cycles of 808 nm laser (0.5 W cm^{-2}) irradiation, while the temperature of ICG was only increased to 38.4 °C. Furthermore, the absorption spectrum of the IEICO NP solution did not show a significant change after 10 min irradiation, while the absorption of the ICG was reduced by 55% (Fig. 2d and Fig. S3, ESI†), and the morphology of the NPs also shows no obvious change after laser irradiation (Fig. S4, ESI†). The above results further verified that the IEICO NPs possess relatively high stability under laser irradiation. On the contrary, the absorption spectra of IEICO in toluene solution shown in Fig. S5 (ESI†) were significantly decreased on prolonging the irradiation time.

Singlet Oxygen Sensor Green® (SOSG) was used to evaluate the $^1O_2$ generation capacity of IEICO NPs because the weak fluorescent SOSG can react with $^1O_2$ quantitatively and rapidly

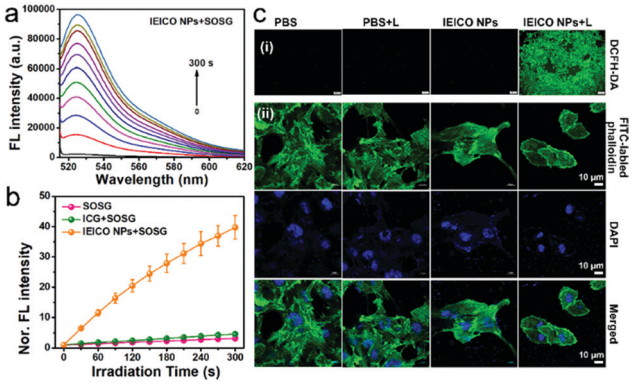

Fig. 3 (a) Time-dependent fluorescence spectra (λ_{ex} = 504 nm) of SOSG in the presence of IEICO NPs after 808 nm laser irradiation (0.02 W cm^{-2}). (b) Time-dependent normalized fluorescence intensity at 530 nm of SOSG in the presence of IEICO NPs (orange dot line), ICG (green dot line), and pure water (red dot line). (c) Fluorescence images of the 4T1 cells stained with (i) DCFH-DA and (ii) FITC-labelled phalloidin, respectively.

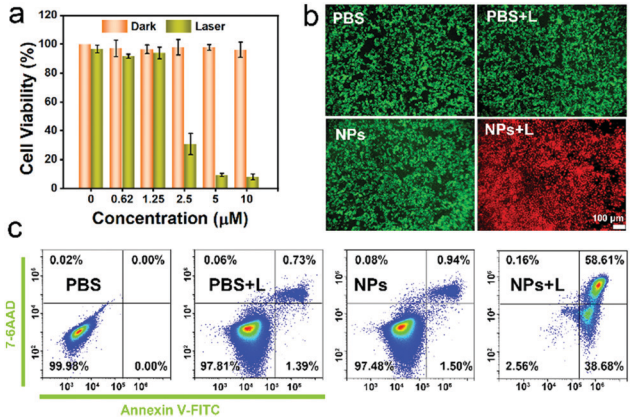

Fig. 4 (a) Cell viability of 4T1 cells treated with different concentrations of IEICO NPs in the dark (yellow bars) or under 808 nm laser irradiation for 10 min (green bars). (b) Calcein AM and PI co-staining of 4T1 cells in different groups. (c) Apoptosis analysis results of annexin V-FITC/7-AAD-stained 4T1 cells.

to produce the oxidation product, which exhibits a strong green fluorescence peak at 530 nm. The irradiation time-dependent fluorescence increases in Fig. 3a and Fig. S6 (ESI†) demonstrated the effective $^1O_2$ generation of the IEICO NPs and IEICO. In addition, the fluorescence intensity of the IEICO NPs + SOSG group at 530 nm was increased by about 40 times compared to the intensity in the other two control groups (Fig. 3b). The $^1O_2$ generation quantum yield was calculated to be 11.0%, which is much higher than that of ICG (only ~0.8%).

Furthermore, 2′,7′-dichlorodihydrofluorescein diacetate (DCFH-DA) was used to evaluate the $^1O_2$ generation capability in living cells. As shown in Fig. 3c(i), only the cells incubated with IEICO NPs and exposed to laser irradiation, *i.e.*, the IEICO NPs + Laser group, showed bright green fluorescence that suggests $^1O_2$ generation. In contrast, the cells only incubated with IEICO NPs, only exposed to laser irradiation, or only added with PBS did not show obvious fluorescence signals. In addition to the $^1O_2$ generation after irradiation, heat production in living cells incubated with IEICO NPs after laser irradiation was also studied. Herein FITC labelled-phalloidin was used to evaluate the photothermal capability of the IEICO NPs in cells. As shown in Fig. 3c(ii), the structure of the IEICO NPs + Laser group was broken after laser irradiation, indicating that laser-induced heat can destroy the cytoskeleton effectively. In contrast, the cytoskeleton in the control groups was rigid and complete. These results demonstrated that the IEICO NPs had a remarkable $^1O_2$ and thermal generation capability in living cells, which is advantageous for their PDT/PTT applications.

An MTT assay was used to quantificationally evaluate the *in vitro* phototherapeutic efficacy and biocompatibility of the IEICO NPs. As revealed in Fig. 4a, the 4T1 cells incubated with different concentrations of IEICO NPs but without laser irradiation exhibited almost 100% cell viability, indicating that the IEICO NPs possess good biocompatibility. On the contrary, when the cells were exposed to laser irradiation, the cell viability was gradually decreased with the increase of the concentration of IEICO NPs, and in the presence of 10 μM IEICO NPs, the cell viability was less than 10%. Furthermore, the Calcein AM and propidium iodide (PI) co-staining assays were carried out to visualize the therapeutic efficacy of the IEICO NPs. As shown in Fig. 4b, strong green fluorescence was detected in the cells after IEICO NP incubation or the laser treatment, revealing that IEICO NPs or laser irradiation cannot induce cell death. However, in the cells incubated with IEICO NPs and then exposed to laser irradiation, a strong red fluorescence signal was observed, suggesting that only the combination of IEICO NPs and laser irradiation can effectively kill cancer cells. These results illustrated that IEICO NPs have excellent biocompatibility and significantly high phototoxicity and can be applied in the phototherapy of cancer. To further understand the mechanism of the cell death induced by IEICO NPs and laser treatment, apoptosis analysis was performed. The quantitative flow cytometric results in Fig. 4c illustrated that the mechanism of cell death is apoptosis and the apoptosis/necrosis rate of the NPs + Laser group was 58.61%. In contrast, the apoptosis rate in other groups was negligible. These results indicated that IEICO NPs and the laser treatment could trigger the apoptosis of cancer cells with $^1O_2$ and heat.

Due to the great photothermal ability of IEICO NPs, the potential application of *in vivo* PA imaging was studied using 4T1 tumor-bearing mice. As shown in Fig. 5a, an obvious PA signal was found after intratumoral injection of IEICO NPs (10 μM). Moreover, the temperature of the tumor injected with IEICO NPs was gradually increased with the laser irradiation time. The intratumor temperature reached up to 59 °C within 8 min (Fig. 5b), which was high enough to achieve thermal tumor ablation. Then, the *in vivo* therapeutic effect of IEICO NPs was further studied. The tumor-bearing mice were divided into four groups (five in each group). The mice in the experimental group were intratumorally injected with IEICO NPs (10 μM) and irradiated with an 808 nm laser. The remaining

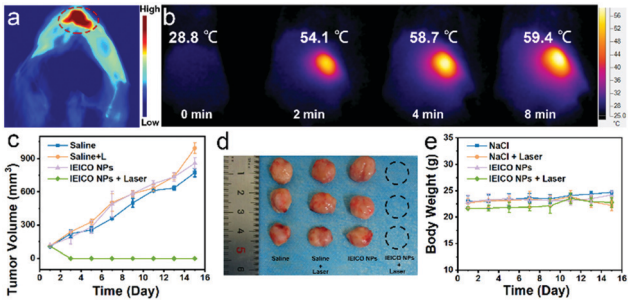

Fig. 5 (a) PA signal of IEICO NPs in 4T1 mice tumors. (b) Infrared thermal images of tumor-bearing mice intratumorally injected with IEICO NPs and exposed to the 808 nm laser irradiation (1 W cm^{-2}). (c) Time-dependent tumor volume. (d) Representative tumor images of different treatment groups after 15 days. (e) Time-dependent body weight variation of the mice during the 15-day treatment.

three experimental groups were given saline, saline + 808 nm laser and IEICO NPs (10 μM), respectively. After different treatments, the tumor volume and body weight of the mice were monitored and recorded for 15 consecutive days. As shown in Fig. 5c and d, the tumor treated with IEICO NPs + Laser was completely ablated without recurrence, while the tumor in the other three groups showed a similar growth trend. In addition, the body weight of the mice in the four groups did not change significantly (Fig. 5e), indicating that all treatments had little systemic toxicity to mice.

To further evaluate the biodistribution and biosafety of IEICO NPs, the enrichment and slicing of organs were conducted. As shown in Fig. S7, (ESI†) IEICO NPs mainly distributed in liver and kidneys after 1 h intravenous injection, and in the liver and spleen after 4 h intravenous injection. However, there is no obvious aggregation in the tumor region. Based on that, the *in vivo* phototherapeutic efficacy of IEICO NPs was investigated by using intratumoral injection. As shown in Fig. 6a, the H&E and Ki67 stained slices of the group treated with Laser alone or IEICO NPs alone showed no difference from those of the PBS group, while the IEICO NPs + Laser group showed obvious damage and proliferation inhibition. Moreover, the H&E staining results of the major organs shown in Fig. 6b also demonstrated the reliable biosafety of IEICO NPs. To further exclude the side effects induced by IEICO NPs, the blood routine analysis was conducted. As shown in Fig. 6c, all the indicators are normal. The above results demonstrated that the obtained IEICO NPs possess relatively high biocompatibility.

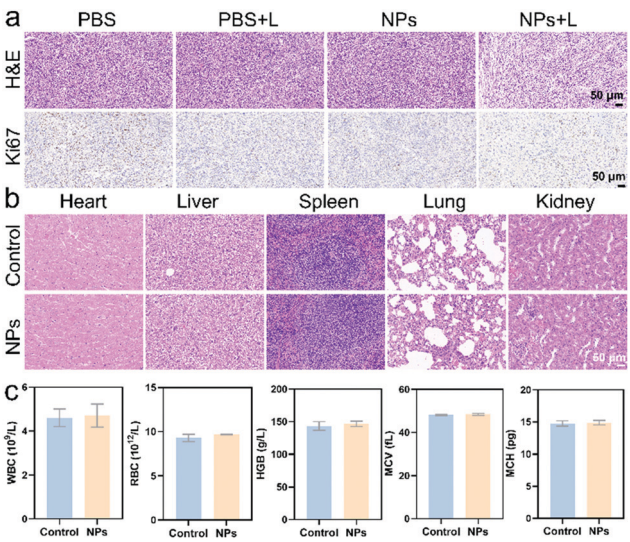

Fig. 6 (a) The H&E and Ki67 staining slices of tumors that received different treatments. (b) The H&E staining of major organs. (c) The blood routine analysis results.

Conclusions

In this work, the star photovoltaic molecule IEICO with strong NIR absorption and narrow bandgap was selected and prepared into water dispersible NPs. The obtained IEICO NPs possess a high $^1O_2$ quantum yield (11%) and PCE (85.4%) under 808 nm laser irradiation. The ultra-high light energy utilization efficacy (96.4%) of IEICO NPs was attributed to their narrow bandgap and large A–D–A conjugated structure, which can bring red-shifted absorbance and relatively high $^1O_2$ generation ability. Both the *in vivo* and *in vitro* experimental results demonstrated the great application potential of IEICO NPs with excellent biocompatibility in PA imaging-guided NIR laser triggered synergetic photodynamic and photothermal therapy. This work expands the application of photovoltaic materials in phototherapy.

Author contributions

K. Yang and Z. Zhang contributed equally to this work; M. Lan planned and supervised the project; K. Yang wrote the whole manuscript; Y. Gan, L. Huang and Q. Tan conducted the preparation of NPs and the photothermal and photodynamic related experiments; Z. Zhang and G. Hu contributed to cell and animal experiments; B. Wang, X. Song and P. Yin contributed to data analysis and article polishing.

Conflicts of interest

There are no conflicts to declare.

Acknowledgements

This work was supported by the National Natural Science Foundation of China (No. 61805287 and 62175262), and the Innovation-Driven Project of Central South University (No. 2020CX021).

Notes and references

1 D. E. Citrin, *N. Engl. J. Med.*, 2017, **377**, 1065–1075.

2 D. De Ruysscher, G. Niedermann, N. G. Burnet, S. Siva, A. W. M. Lee and F. Hegi-Johnson, *Nat. Rev. Dis. Primers*, 2019, **5**, 13.
3 G. Song, L. Cheng, Y. Chao, K. Yang and Z. Liu, *Adv. Mater.*, 2017, **29**, 1700996.
4 B. L. Li, S. J. Zhao, L. Huang, Q. Wang, J. F. Xiao and M. H. Lan, *Chem. Eng. J.*, 2020, **408**, 127245.
5 X. Li, J. F. Lovell, J. Yoon and X. Chen, *Nat. Rev. Clin. Oncol.*, 2020, **17**, 657–674.
6 X. Li, N. Kwon, T. Guo, Z. Liu and J. Yoon, *Angew. Chem., Int. Ed.*, 2018, **57**, 11522–11531.
7 M. Lan, S. Zhao, W. Liu, C.-S. Lee, W. Zhang and P. Wang, *Adv. Healthcare Mater.*, 2019, **8**, 1900132.
8 L. Huang, D. Qing, S. Zhao, X. Wu, K. Yang, X. Ren, X. Zheng, M. Lan, J. Ye, L. Zeng and G. Niu, *Chem. Eng. J.*, 2022, **430**, 132638.
9 Y. Liu, P. Bhattarai, Z. Dai and X. Chen, *Chem. Soc. Rev.*, 2019, **48**, 2053–2108.
10 J. Chen, C. Ning, Z. Zhou, P. Yu, Y. Zhu, G. Tan and C. Mao, *Prog. Mater. Sci.*, 2019, **99**, 1–26.
11 S. Liu, X. Pan and H. Liu, *Angew. Chem., Int. Ed.*, 2020, **59**, 5890–5900.
12 X. Deng, Z. Shao and Y. Zhao, *Adv. Sci.*, 2021, **8**, 2002504.
13 K. Yang, S. Zhao, B. Li, B. Wang, M. Lan and X. Song, *Coord. Chem. Rev.*, 2022, **454**, 214330.
14 G. Hong, S. Diao, A. L. Antaris and H. Dai, *Chem. Rev.*, 2015, **115**, 10816–10906.
15 J. Jia, G. Liu, W. Xu, X. Tian, S. Li, F. Han, Y. Feng, X. Dong and H. Chen, *Angew. Chem., Int. Ed.*, 2020, **59**, 14443–14448.
16 R. R. Nasaruddin, T. Chen, Q. Yao, S. Zang and J. Xie, *Coord. Chem. Rev.*, 2021, **426**, 213540.
17 T. A. Tabish, P. Dey, S. Mosca, M. Salimi, F. Palombo, P. Matousek and N. Stone, *Adv. Sci.*, 2020, **7**, 1903441.
18 S. He, J. Song, J. Qu and Z. Cheng, *Chem. Soc. Rev.*, 2018, **47**, 4258–4278.
19 X. Li, F. Fang, B. Sun, C. Yin, J. Tan, Y. Wan, J. Zhang, P. Sun, Q. Fan, P. Wang, S. Li and C.-S. Lee, *Nanoscale Horiz.*, 2021, **6**, 177–185.
20 Q. Wang, Y. Dai, J. Xu, J. Cai, X. Niu, L. Zhang, R. Chen, Q. Shen, W. Huang and Q. Fan, *Adv. Funct. Mater.*, 2019, **29**, 1901480.
21 C. Zhao, J. Wang, X. Zhao, Z. Du, R. Yang and J. Tang, *Nanoscale*, 2021, **13**, 2181–2208.
22 Y. Cui, H. Yao, L. Hong, T. Zhang, Y. Xu, K. Xian, B. Gao, J. Qin, J. Zhang, Z. Wei and J. Hou, *Adv. Mater.*, 2019, **31**, 1808356.
23 T. Zhang, X. Zhao, D. Yang, Y. Tian and X. Yang, *Adv. Energy Mater.*, 2018, **8**, 1701691.
24 C. H. Duan, K. Zhang, C. M. Zhong, F. Huang and Y. Cao, *Chem. Soc. Rev.*, 2013, **42**, 9071–9104.
25 Y. Lin, Z.-G. Zhang, H. Bai, J. Wang, Y. Yao, Y. Li, D. Zhu and X. Zhan, *Energy Environ. Sci.*, 2015, **8**, 610–616.
26 H. Yao, Y. Chen, Y. Qin, R. Yu, Y. Cui, B. Yang, S. Li, K. Zhang and J. Hou, *Adv. Mater.*, 2016, **28**, 8283–8287.
27 S. Tian, H. Bai, S. Li, Y. Xiao, X. Cui, X. Li, J. Tan, Z. Huang, D. Shen, W. Liu, P. Wang, B. Z. Tang and C.-S. Lee, *Angew. Chem., Int. Ed.*, 2021, **60**, 1–6.
28 S. L. Higgins and K. J. Brewer, *Angew. Chem., Int. Ed.*, 2012, **51**, 11420–11422.
29 Y. Li, G. Xu, C. Cui and Y. Li, *Adv. Energy Mater.*, 2018, **8**, 1701791.
30 Z. G. Zhang, Y. Yang, J. Yao, L. Xue, S. Chen, X. Li, W. Morrison, C. Yang and Y. Li, *Angew. Chem., Int. Ed.*, 2017, **56**, 13503–13507.
31 J. Chen, K. Wen, H. Chen, S. Jiang, X. Wu, L. Lv, A. Peng, S. Zhang and H. Huang, *Small*, 2020, **16**, 2000909.
32 Y. P. Wan, G. H. Lu, W. C. Wei, Y. H. Huang, S. L. Li, J. X. Chen, X. Cui, Y. F. Xiao, X. Z. Li, Y. H. Liu, X. M. Meng, P. F. Wang, H. Y. Xie, J. F. Zhang, K. T. Wong and C. S. Lee, *ACS Nano*, 2020, **14**, 9917–9928.
33 U. Bilati, E. Allemann and E. Doelker, *Eur. J. Pharm. Sci.*, 2005, **24**, 67–75.
34 Z. Guo, H. He, Y. Zhang, J. Rao, T. Yang, T. Li, L. Wang, M. Shi, M. Wang, S. Qiu, X. Song, H. Ke and H. Chen, *Adv. Mater.*, 2021, **33**, 2004225.
35 H. He, S. Ji, Y. He, A. Zhu, Y. Zou, Y. Deng, H. Ke, H. Yang, Y. Zhao, Z. Guo and H. Chen, *Adv. Mater.*, 2017, **29**, 1606690.
36 D. Xi, M. Xiao, J. Cao, L. Zhao, N. Xu, S. Long, J. Fan, K. Shao, W. Sun, X. Yan and X. Peng, *Adv. Mater.*, 2020, **32**, 1907855.
37 J. Zhao, K. Xu, W. Yang, Z. Wang and F. Zhong, *Chem. Soc. Rev.*, 2015, **44**, 8904–8939.